Electronic Supplementary Material (ESI) for Journal of Materials Chemistry A.

Supplementary Information

Improved Hydrogen Oxidation Reaction in Alkaline Condition by Ruthenium-Iridium Alloyed Nanoparticles

Junya Ohyama,[a,b*] Daiki Kumada,[a] Atsushi Satsuma[a,b]

[a] *Graduate School of Engineering, Nagoya University, Nagoya 464-8603, Japan.*

[b] *Elements Strategy Initiative for Catalysts and Batteries (ESICB), Kyoto University, Katsura, Kyoto 615-8520, Japan.*

Correspondence - ohyama@apchem.nagoya-u.ac.jp

EXAFS analysis of Ru-Ir/C-20

Figure S1 and S2 show the Ir L_3 edge and Ru K edge EXAFS spectra of Ru-Ir/C-20. The spectra were obtained on the BL01B1 beamline of SPring-8 (Hyogo, Japan) using a Si(111) two-crystal monochromator for the Ir L_3 edge spectrum, and a Si(311) for the Ru K edge spectrum. Data reduction was performed using REX2000 program ver. 2.5.9 (Rigaku Co.). The k_3 weighted EXAFS oscillations were Fourier transformed in the range of 3 – 15 A^{-1}. The inverse Fourier transformation was carried out in the range of ca. 1.4 – 3.1 Å for the Ir L_3 edge spectrum and ca. 1.3 – 2.9 Å for the Ru K edge spectrum. The curve fitting analysis was performed using theoretical parameters.[1]

The Ir L_3 edge EXAFS of Ru-Ir/C-20 was fitted well using three paths of Ir-Ru, Ir-Ir, and Ir-O, but not using two paths of Ir-Ir and Ir-O without Ir-Ru. The Ru K edge EXAFS was also fitted well with three paths of Ru-Ru, Ru-Ir, and Ru-O, but not without Ru-Ir. The results suggest the formation of Ru-Ir alloy in Ru-Ir/C-20. The structural parameters obtained from the curve fitting analysis of the Ir L_3 edge spectrum and those from Ru K edge spectrum are summarized Table S1 and S2, respectively.

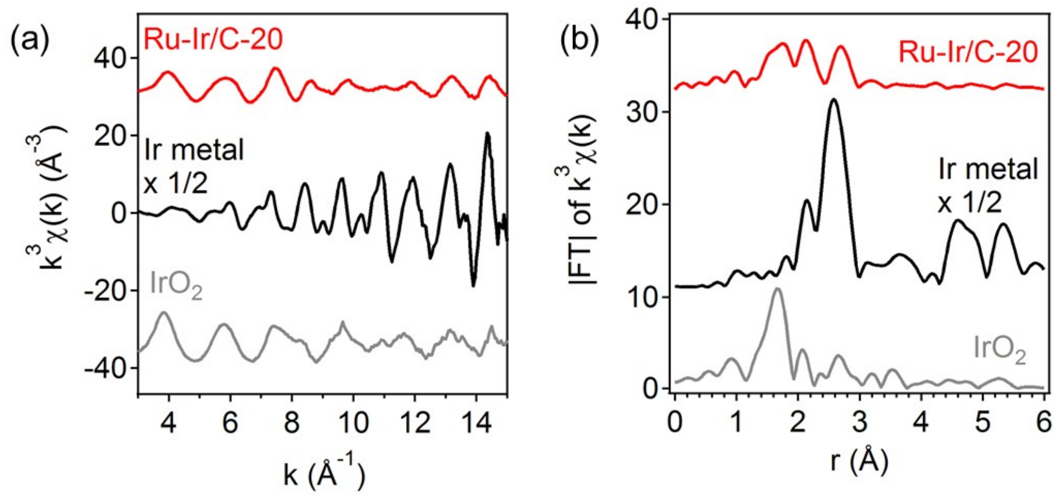

Figure S1. (a) The Ir L_3 edge EXAFS spectrum of Ru-Ir/C-20 together with those of Ir metal powder and IrO_2; (b) their Fourier transforms.

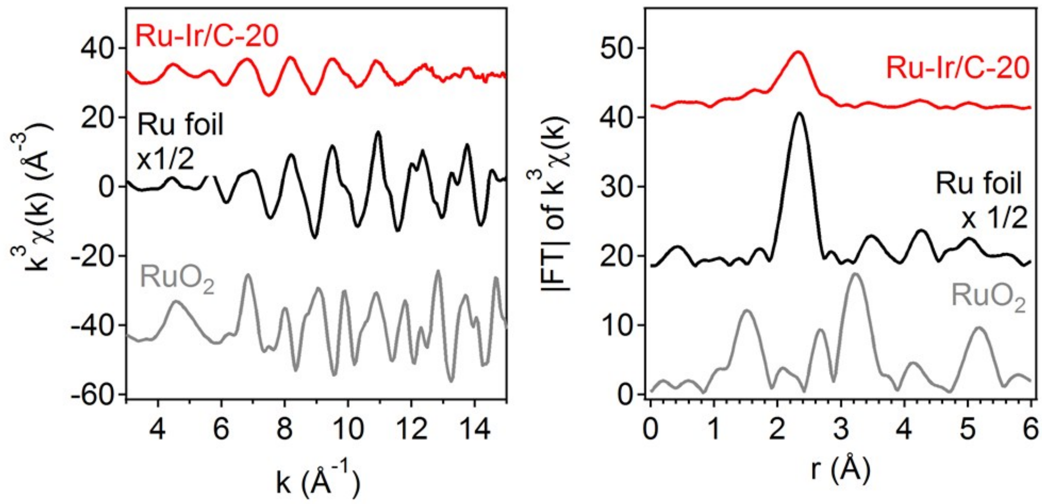

Figure S2. (a) The Ru K edge EXAFS spectrum of Ru-Ir/C-20 together with those of Ru foil and RuO_2; (b) their Fourier transforms.

Table S1. Structural parameters of Ru-Ir/C-20 obtained from the curve fitting analysis of the Ir L_3 EXAFS spectrum.

$R_{Ir\text{-}Ru}$ (Å)	$N_{Ir\text{-}Ru}$	$R_{Ir\text{-}Ir}$ (Å)	$N_{Ir\text{-}Ir}$	$R_{Ir\text{-}O}$ (Å)	$N_{Ir\text{-}O}$
2.67 ± 0.02	2.7 ± 1.5	2.73 ± 0.01	3.0 ± 0.9	1.99 ± 0.02	1.9 ± 0.4

Table S2. Structural parameters of Ru-Ir/C-20 obtained from the curve fitting analysis of the Ru K edge EXAFS spectrum.

$R_{Ru\text{-}Ir}$ (Å)	$N_{Ru\text{-}Ir}$	$R_{Ru\text{-}Ru}$ (Å)	$N_{Ru\text{-}Ru}$	$R_{Ru\text{-}O}$ (Å)	$N_{Ru\text{-}O}$
2.67 ± 0.05	2.41 ± 1.7	2.66 ± 0.01	3.11 ± 13	1.97 ± 0.08	0.35 ± 0.5

Cu_{upd} stripping voltammograms

Figures S3-S8 show the Cu_{upd} stripping voltammograms of the catalysts. The (total) ECSA was determined from the charge of Cu_{upd} stripping after deposition at 0.3 V vs. RHE ($Q_{0.3}$) using a conversion factor of 420 μC cm^{-2}.[2-4] In the case of Ru-Ir/C, the ECSA of Ir was calculated using the charge of Cu_{upd} stripping after deposition at 0.45 V vs. RHE ($Q_{0.45}$): ECSA of Ir = $xQ_{0.45}/420/w_{catal}$, where x is the correction factor calculated by $Q_{0.3}/Q_{0.45}$, and w_{catal} is the weight of Ru-Ir/C on the disk (1.96 μg). The ECSA of Ru in Ru-Ir/C was calculated by subtraction of ECSA of Ir from total ECSA.

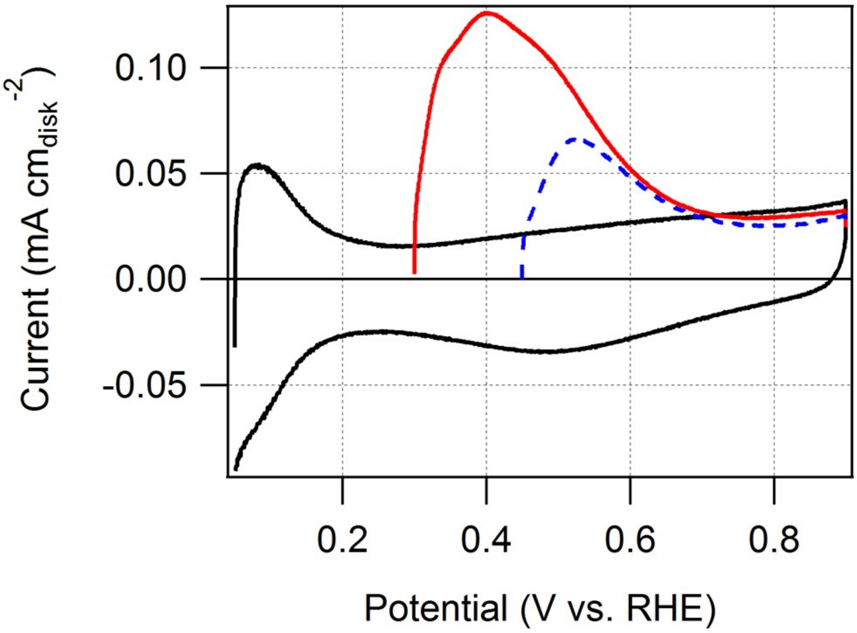

Figure S3. Cu_{upd} striping voltammograms of Ru-Ir/C-20 after Cu deposition at 0.3 V (red solid) and 0.45 V vs. RHE (blue dashed), together with a CV of Ru-Ir/C-20 obtained in the absence of $CuSO_4$ (black solid). The ECSA of Ru+Ir was determined from $Q_{0.3}$. The ECSA of only Ir was calculated using $Q_{0.45}$ as described above, because the Cu deposition does not occur on Ru at 0.45 V but does on Ir as shown in Figures S5 and S6.

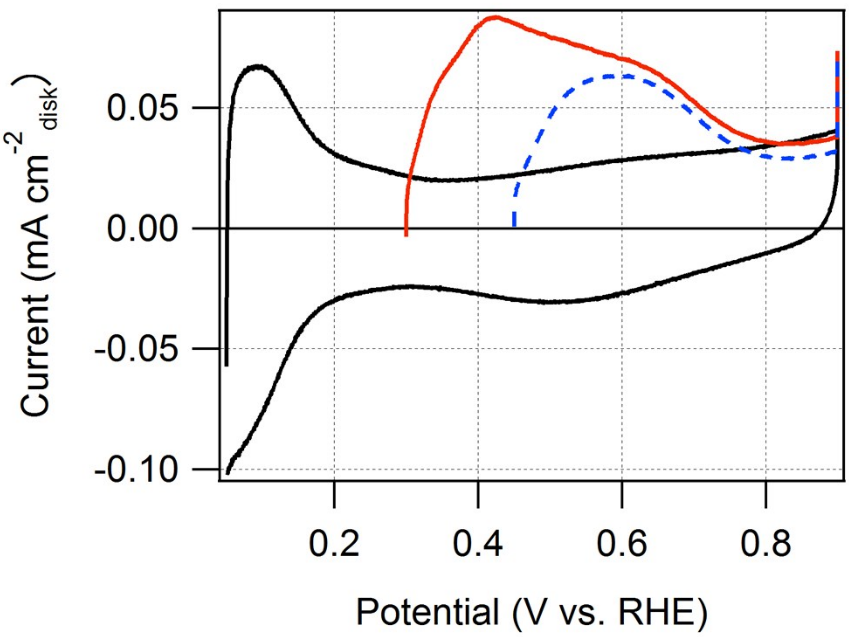

Figure S4. Cu_{upd} striping voltammograms of Ru-Ir/C-60 after Cu deposition at 0.3 V (red solid) and 0.45 V vs. RHE (blue dashed), together with a CV of Ru-Ir/C-60 obtained in the absence of $CuSO_4$ (black solid).

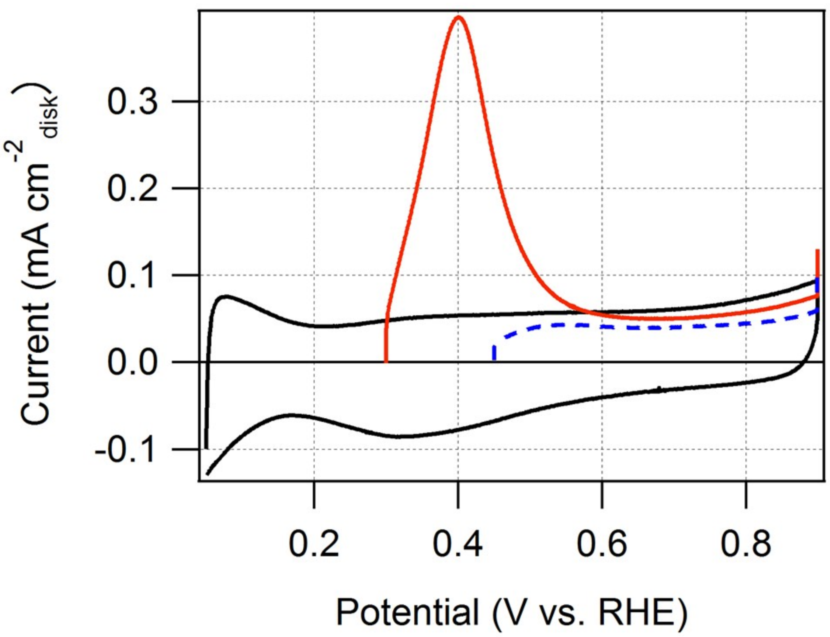

Figure S5. Cu_{upd} striping voltammograms of Ru/C after Cu deposition at 0.3 V (red solid) and 0.45 V vs. RHE (blue dashed), together with a CV of Ru/C obtained in the absence of $CuSO_4$ (black solid). The voltammogram from 0.45 V shows no current due to no deposition of Cu at 0.45 V.

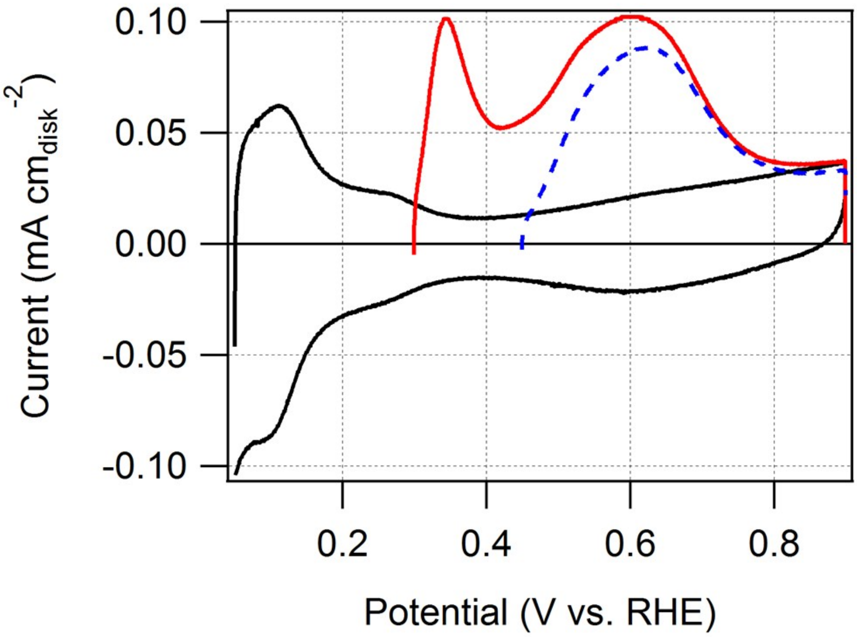

Figure S6. Cu_{upd} striping voltammograms of Ir/C after Cu deposition at 0.3 V (red solid) and 0.45 V vs. RHE (blue dashed), together with a CV of Ir/C obtained in the absence of $CuSO_4$ (black solid). The voltammogram from 0.45 V shows the current due to Cu_{upd} stripping, and was similar to that from 0.3 V.

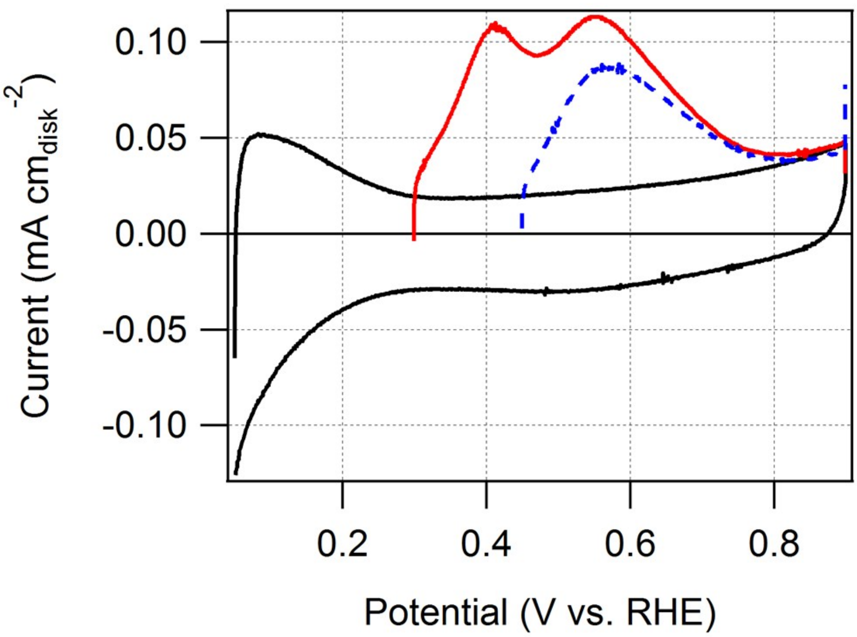

Figure S7. Cu_{upd} striping voltammograms of Pt-Ru/C after Cu deposition at 0.3 V (red solid) and 0.45 V vs. RHE (blue dashed), together with a CV of Pt-Ru/C obtained in the absence of $CuSO_4$ (black solid). The ECSAs of Pt+Ru and only Pt were determined by the same method used for Ru-Ir/C.

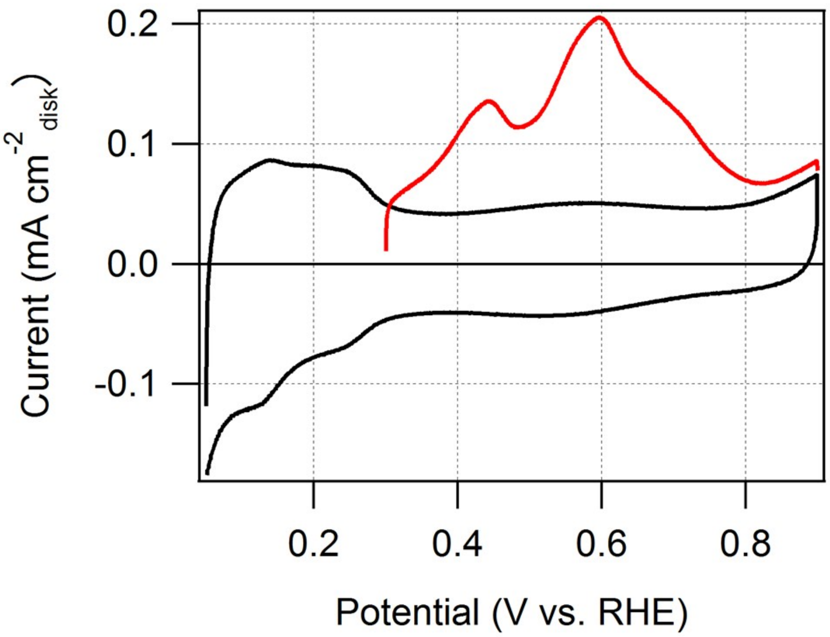

Figure S8. Cu_{upd} striping voltammograms of Pt/C after Cu deposition at 0.3 V (red solid), together with a CV of Pt/C obtained in the absence of $CuSO_4$ (black solid) as a back ground.

Specific activities

The exchange current density (i_0) of Pt/C was evaluated using two fitting methods: the Butler-Volmer method shown in Figure S9; the micropolarization method described in the main text. Then, the specific activity (SA) of Pt/C was calculated by normalization of i_0 by the ECSA evaluated from H_{upd} and Cu_{upd}. The result is presented in the entries 1 and 2 of Table S3. The SAs of Pt/C obtained in this study are similar to the literature values. The SAs of the catalysts using in this study were listed in Table S4. The SAs in Table S4 were evaluated using the micropolarization method and the Cu_{upd} ECSA.

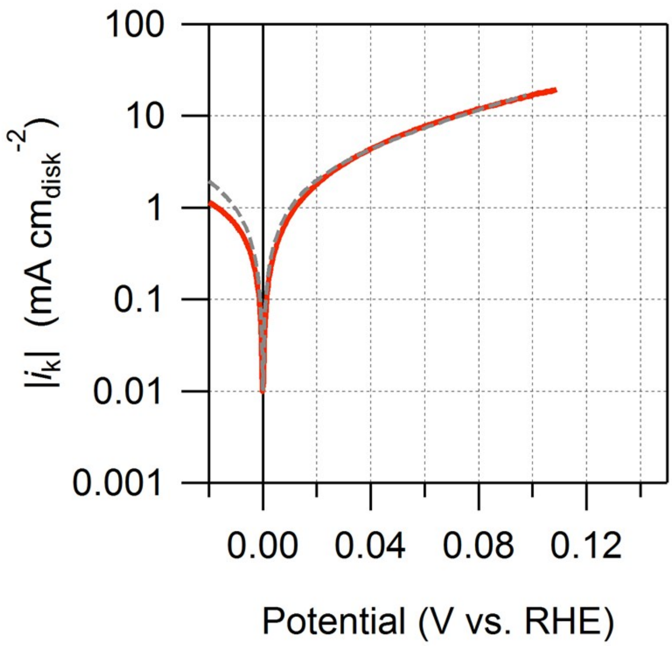

Figure S9. The kinetic current density (i_k) on Pt/C (red solid) with a fitting (grey dashed) using the Butler-Volmer equation: $i_k = i_0\,(e^{\frac{\alpha F\eta}{RT}} - e^{\frac{-(1-\alpha)F\eta}{RT}})$, where η is the overpotential, α the transfer coefficient, T the temperature (298 K), R the gas constant (8.314 J mol^{-1} K^{-1}), and F the Faraday constant (96485 A s mol^{-1}).

Table S3. The specific activities of Pt/C evaluated in this study and those in the literature.

Entry	Reference	ECSA ($m^2\ g_{Pt}^{-1}$)	Temp. (K)	SA ($mA\ cm_{Pt}^{-1}$)
1[a]	This study	52[c]	298	0.50[e], 0.33[f]
2[a]		92[d]		0.28[e], 0.18[f]
3[b]	*J. Electrochem. Soc.* 2010, **157**, B1529 (ref. 5)	62[c]	294	0.57[e]
4[b]	*Sci. Adv.* 2016, **2**, e1501602 (ref. 6)	64[c]	293	0.46[e]
5[a]	*J. Phys. Chem. C* 2015, **119**, 13481 (ref. 7)	54[d]	r.t.	0.49[e]
6[a]	*Energy. Environ. Sci.* 2014, **7**, 2255 (ref. 8)	120[c]	313	1.2[e], 0.8[f]

[a] in 0.1 M NaOH, [b] in 0.1 M KOH, [c] from H_{upd}, [d] from Cu_{upd}, [e] Butler-Volmer method, [f] micropolarization method.

Table S4. The SAs of the catalysts used in this study. [a]

Catalyst	Cu_{upd} ECSA ($m^2\ g_{metal}^{-1}$)	SA ($mA\ cm_{metal}^{-1}$)
Ru-Ir/C-20	72	0.85
Ru-Ir/C-60	70	0.56
Ru/C	101	0.18
Ir/C	65	0.30
Pt-Ru/C	67	0.60
Pt/C	92	0.18

[a] The SAs were evaluated using the micropolarization method and the ECSAs evaluated by the Cu_{upd} method.

References

1. A. G. McKale, B. W. Veal, A. P. Paulikas, S. K. Chan and G. S. Knapp, *J. Am. Chem. Soc.*, 1988, **110**, 3763.
2. C. L. Green and A. Kucernak, *J. Phys. Chem. B*, 2002, **106**, 1036.
3. C. L. Green and A. Kucernak, *J. Phys. Chem. B*, 2002, **106**, 11446.
4. T. Onodera, S. Suzuki, Y. Takamori and H. Daimon, *Appl. Catal., A*, 2010, **379**, 69.
5. W. Sheng, H. A. Gasteiger and Y. Shao-Horn, *J. Electrochem. Soc.* 2010, **157**, B1529.
6. J. Zheng, W. Sheng, Z. Zhuang, B. Xu and Y. Yan, *Sci. Adv.* 2016, **2**, e1501602.
7. S. St. John, R. W. Atkinson, R. R. Unocic, T. A. Zawodzinski and A. B. Papandrew, *J. Phys. Chem. C* 2015, **119**, 13481.
8. J. Durst, A. Siebel, C. Simon, F. Hasche, J. Herranz and H. A. Gasteiger, *Energy. Environ. Sci.* 2014, **7**, 2255.